Ion-irradiation-induced stresses and swelling in amorphous Ge thin films

S. G. Mayr[1,2,*] and R. S. Averback[2]
[1]*I. Physikalisches Institut, Universität Göttingen, Friedrich-Hund-Platz 1, 37077 Göttingen, Germany*
[2]*Department of Materials Science and Engineering and Frederick Seitz Materials Research Laboratory, University of Illinois at Urbana-Champaign, Urbana, Illinois 61801, USA*
(Received 16 November 2004; published 5 April 2005)

Mechanical stresses and morphology during growth and ion bombardment of amorphous Ge thin films are investigated by a combination of *in situ* stress measurements and molecular dynamics computer simulations. Strong compressive stresses are generated during irradiation that subsequently lead to severe swelling. The simulations indicate that interstitial-mediated viscous flow in combination with well-localized vacancy defects are the main ingredients responsible for the observed phenomena.

DOI: 10.1103/PhysRevB.71.134102 PACS number(s): 61.43.Dq, 61.80.Jh, 61.82.Bg

I. INTRODUCTION

Stress evolution in amorphous thin films has been of sustained scientific interest since the pioneering works of Bauer and Buckel.[1] This interest is often motivated by the fact that stresses reflect the internal structure and surface morphology of thin films, and hence they provide a useful monitor of surface and bulk processes, as well as structural changes. In addition, large stresses in these films can often lead to thin film failure, such as growth instabilities, film decohesion, or crack formation (see Ref. 2 for an overview). Most previous work on amorphous films has focused on stress generation and surface morphology during vapor deposition of metallic alloys[3,4] and elemental semiconductors.[5] Stresses in these situations are often as large as several GPa. Clearly, under the low-mobility growth conditions required to grow an amorphous film, the mechanism underlying the growth morphology are strongly linked to the energetics and atomic-scale kinetics at the open surface, i.e., surface energy and stress, surface diffusion, and plasticity.[4] Stress evolution in covalently bonded amorphous systems is less well understood than in metals, especially in the late stages of film growth (i.e., thicknesses of several hundred nanometers). The present work is concerned with altering the stress and morphology in these amorphous thin films by ion bombardment, as shown possible for metallic[6,7] and SiO_2 glasses,[8] and also during radiation-induced amorphization of Si.[9] In the case of metallic glasses, we identified radiation-induced viscous flow as the origin of stress relaxation at low doses and mass flow onto the surface as the cause of stress generation at higher doses.[7] Using molecular dynamics computer simulations we also identified radiation-induced point defects in the amorphous metal, i.e., vacancies and interstitials, as the atomic-scale entities that are responsible for mediating plastic deformation.[10] The present work addresses whether these same mechanisms apply as well to covalently bonded systems, where phenomena not found in metals are known to occur.

The present investigation employs mechanical stress measurements as well as atomic force microscopy (AFM) to investigate stress and morphology evolution in *thick* amorphous Ge (*a*-Ge) films during growth from the vapor and during subsequent MeV ion bombardment. The choice of Ge is motivated by the fact that *a*-Ge is representative of a class of covalently bonded materials that are known to exhibit strong anomalies in comparison to metals, such as *compressive* surface stress, *contraction* during melting and swelling during ion bombardment. In fact, the enormous swelling in *a*-Ge during ion bombardment is a phenomenon that was discovered over 20 years ago,[11–19] but one that remains largely unexplained. It is the aim of the present paper to investigate the role of stresses and their relation to the morphology of the film and swelling. We do this through a combination of experimental and large-scale molecular dynamics simulations.

II. EXPERIMENTAL AND SIMULATIONAL METHODS

Amorphous Ge films were condensed from an electron beam evaporator onto $\approx 200\ \mu$m thick naturally oxidized Si(100) wafers at a deposition rate of ≈ 5 Å/s under UHV conditions. Biaxial intrinsic growth stresses σ were obtained using the modified Stoney equation[20] and *in situ* substrate curvature measurements that employed a two laser-beam deflection method.[4] Ion beam irradiations were performed under HV conditions using a rastered Kr^+ ion beam at 1.8 MeV for samples designated for *ex situ* surface characterization. Irradiation induced stress changes were monitored by substrate curvature measurements using a three capacitor dilatometer; details of the apparatus can be found elsewhere.[21] An ion energy of 700 keV was selected for these samples to prevent ion beam mixing at the film/substrate interface, while maintaining a maximum thickness of the film affected by ion bombardment. The irradiated portion of the Ge films was determined from the damage distribution, obtained from SRIM,[45] using a cutoff of e^{-1} of the maximum damage. For the conversion of fluences to doses [measured in displacements per atoms (dpa)] a displacement energy of 15 eV was assumed.[22]

The surface topographies of the samples were characterized *ex situ* using a commercial atomic force microscope (AFM) in contact and tapping mode. The surface morphology data is evaluated by calculating the root mean square surface roughness ξ. Additionally, a profilometer was used to measure radiation induced changes of the film thickness

within an irradiated spot, relative to the surrounding sample. Radiation induced swelling perpendicular to the substrate was characterized by the strain ϵ_{zz}, which is determined by normalizing the increase in film thickness to the effectively irradiated portion of the film, taking sputtering into account (surface binding energy, 3.88 eV). Amorphicity was verified by x-ray diffraction using a Cu Kα source; none of the samples showed indications of crystallization. For *as grown* films at room temperature, this conclusion had been reached previously.[23]

Classical molecular dynamics (MD) simulations were performed using PARCAS.[24] Two different types of potentials were employed to examine the sensitivity of the results to the choice of potential. The Tersoff potential[25,26] with λ_3 correction (*T*-Ge) was used primarily in the present study due to its ability to correctly describe a variety of bonding environments,[27] which is of special importance for the amorphous state. Its main drawback, however, is its prediction of an unrealistically high melting temperature[28] $T_M \approx 3300$ K, in comparison to the experimental value ($T_M = 1212$ K). We therefore also used a modified version of the Stillinger-Weber-type potential (SW-Ge),[29–31] which yields a more realistic $T_M \approx 1230$ K (in comparison to $T_M = 2900$ K of the original version), but at the cost of showing deviations in the structural short-range order in the amorphous and liquid state. From the nature of the potentials it is generally expected that SW-Ge has a stronger tendency for tetrahedral bonding than does *T*-Ge.[32] The short-range interactions, which are important for energetic recoils, are described in both our *T*-Ge and SW-Ge potentials by a repulsive potential that was obtained using *ab initio* calculations.[31] The amorphous simulation cells were obtained by quenching from the liquid at constant pressures and quenching rates ν using Berendsen pressure and temperature controls,[33] with periodic boundaries applied in all spatial directions.

Ion irradiation was simulated by successively assigning randomly oriented velocities of the specified kinetic energy to randomly selected target atoms, while maintaining either (a) an open film geometry, with open boundaries in $\pm z$ directions, and fixed periodic boundaries in the $\pm x$ and $\pm y$ directions, or (b) a bulk geometry with fixed periodic boundaries in all spatial directions. These geometries allow for investigations of surface induced effects in the one case, and a direct comparison of recoils with point defects in the other (as seen below). Electronic stopping was incorporated as a frictional force affecting all atoms with a kinetic energy exceeding 10 eV; it was based on the SRIM stopping powers. Significant heating of the simulation cell was prevented by scaling the cell size to the recoil energy and maintaining at least 25 atoms per one eV of recoil energy. The outermost three layers at periodic boundaries of the simulation cells were damped to the desired temperature to imitate the heat flow to an infinite surrounding solid; the strength of the temperature coupling was chosen in a way to minimize reflection of shock waves at the boundaries. As first pointed out over fifty years ago,[34] recoils can produce a thermal spike in densely packed matter. To identify the possibility of local melting near the recoils, a simple kinetic analysis was performed, which labels an atom as "liquid," once the kinetic energy of it and its neighbors exceeds $\frac{3}{2}kT_G$ for at least 10 lattice vibrations. Here T_G denotes the glass transition temperature, which had been determined in a separate simulation on quenching with a comparable cooling rate and pressure.

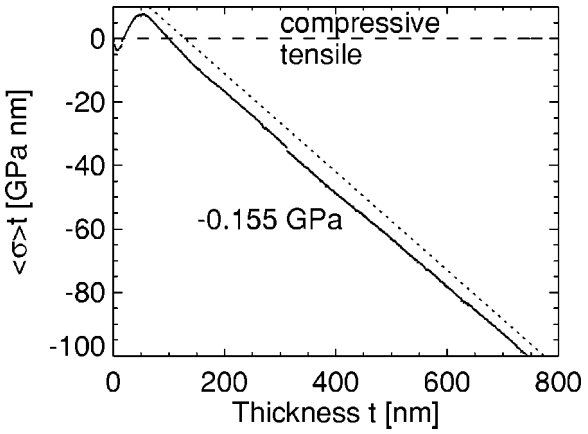

FIG. 1. Force per unit width $\langle\sigma\rangle \cdot t$ during condensation of amorphous Ge films onto oxidized Si (100) substrates (deposition rate: 5 Å/s), as measured by *in situ* curvature measurments. Negative and positive values of the slope correspond to the generation of tensile and compressive stresses, respectively.

Recoil events produce point defects as well as thermal spikes in matter.[35] To distinguish the effects of these two phenomena, an additional type of simulation was performed, where point defects are inserted into the amorphous matrix, either interstitials and vacancies, separately, or as Frenkel pairs; the usefulness of this approach was shown previously.[10] In the case of interstitial insertion, one atom in the amorphous matrix was replaced by two, after locating the minimum energy arrangement of the pair. This procedure ensures that the interstitial formation energy does not exceed 5 eV. In contrast to the simulations of recoils, point defect insertion is not accompanied by significant heat release, and thus it can be performed using small simulation cells, several 10 000's of atoms, with concurrent temperature and pressure controls enabled. This provides for a significant speed-up of the simulations, and thus the treatment of a large number of displacements per atom could be achieved.

III. STRESSES DURING Ge FILM GROWTH

Biaxial stress evolution during growth of *a*-Ge films from vapor shows a close similarity to that of metallic glassy films,[4] suggesting common mechanisms are at play. As seen in Fig. 1, the early stages of growth at room temperature are characterized by the generation of tensile stresses, which is followed by a compressive region. These results are in agreement with those reported by Floro *et al.*[5] As in amorphous metallic alloys, the tensile stresses at very low thicknesses are due to coalescence phenomenon of islands, and the subsequent compressive stress generation to surface reconstruction. In the thick-film regime, starting at ≈ 50 nm, we observe a continuous generation of tensile stresses and a strongly increased surface roughness. This behavior is in direct accord with amorphous metal-alloy thin films, for which the behavior was attributed to a continuous generation and

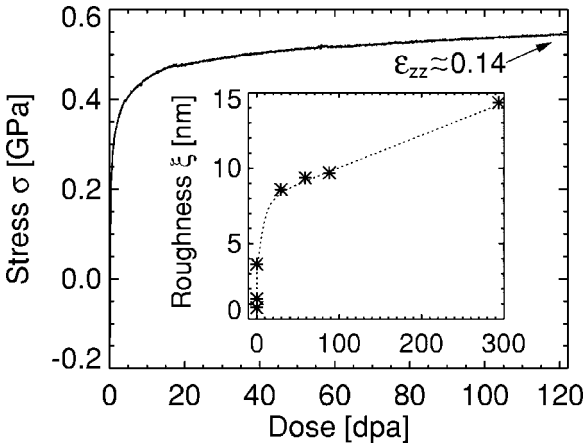

FIG. 2. During bombardment of 510-nm-thick as-grown Ge films with 700 keV Kr^+ ions, compressive stresses are generated, accomanied by a normal strains ϵ_{zz}. Concurrently, the roughness ξ of AFM surface topographs shows a strong increase with dose (inset).

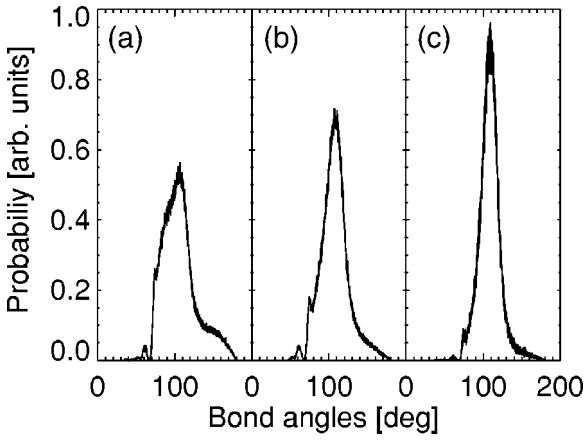

FIG. 3. Comparison of the angular distribution functions ($T=10$ K) of (a) as quenched ($P=4$ GPa), (b) irradiated (0.9 dpa at 5.0 keV), and (c) as quenched ($P=0$ GPa) samples in perodic film geometry.

coalescence of growth columns. It was proposed, that the resulting stress is linked to the size R_C of the columnlike morphology by the equation $\sigma=6\gamma/R_C$, where γ denotes the surface energy.[4] We presently surmise that this expression also holds for the case of *a*-Ge. Unfortunately, a quantitative verification suffers from the lack of a reliable estimate of the surface energy. Our MD simulations using *T*-Ge show that the surface energy can vary by several orders of magnitude, depending on the microstructure of the *a*-Ge. Additionally we expect that a porous microstructure, which has been observed by electron microscopy,[36] contributes a tensile stress due to the surface stress of the pores.

IV. STRESSES AND MORPHOLOGY EVOLUTION IN Ge DURING Mev Kr IRRADIATION

The samples employed in our irradiation studies were described in Secs. II and III. Initially, these samples had a homogeneous stress of $\sigma\approx-0.155$ GPa in the region of the film (Fig. 1) affected by 700 keV Kr^+ irradiation. Ion bombardment dramatically alters the stresses in the film, increasing it nearly exponentially toward a saturation compressive stress of ≈0.6 GPa. This behavior is accompanied by a dramatic increase in the surface roughness, which after an initial rapid transient increases nearly linearly, as shown in the inset of Fig. 2. The measurement of the change in thickness of the irradiated region of the film, or strain ϵ_{zz}, shows that extensive swelling has taken place. Swelling of Ge samples under ion bombardment, in fact, has been extensively reported in the literature under various irradiation conditions.[11–19] Scanning electron microscopy (SEM) and transmission electron microscopy (TEM) investigations reveal a swamplike porous microstructure in the sample. With prolonged sputtering of surface layers, these pores come to dominate the surface roughness, i.e., the roughness shown in Fig. 2 can be regarded as a direct measure of the porosity, or swelling, of the sample. Comparing the generation stress with swelling (roughness), it is seen that the stresses increase much faster than the swelling in the low dose regime, but then more slowly in the high dose regime.

V. MD SIMULATION OF RECOILS IN *a*-Ge

The MD simulation cells for both *a*-*T*-Ge and *a*-SW-Ge were prepared by quenching liquid Ge from 6000 K to 10 K at variable quenching rates and pressures. As shown in previous experiments[37,38] and simulations,[28,39] the quenched-in structure of covalently bonded systems depends strongly on pressure and temperature during the quench. Since some of these previous results are inconsistent, and since the rate *and* pressure during the quench both play a major role, we explored the relationship between the quench conditions and the amorphous structure more thoroughly. The bond angle distribution function (Fig. 3) is particularly insightful for this purpose, although the atomic volume and the pair correlation function, also provide key information.

On quenching the simulation cells, the effect of pressure on the angular distribution function first becomes significant at temperatures as high as 3500 K. At low or negative pressures, a sharp maximum appears at the tetrahedral angle, but it successively broadens as the hydrostatic pressure is increased. The tendency for tetrahedal bonds, moreover, increases on further cooling, and higher pressures are then required to induce deviations from this configuration. The simulations also show that the viscosity of the melt is an increasing function of the number of tetrahedal arrangements. In contrast to simple liquids, therefore, the viscosity decreases with increasing pressure since pressure reduces the fraction of tetrahedal configurations. As an example, we find that in the supercooled liquid region of *a*-*T*-Ge ($T=2200$ K) an increase in pressure from −2 to 2 GPa is capable of reducing the viscosity a factor of ≈2. The structure of the amorphous phase becomes frozen in the simulations when the time for internal relaxation of the supercooled liquid reaches the time scale of the simulation run. Thus it becomes clear that the glass transition at higher pressures (reduced viscosities) occurs at lower temperatures than at

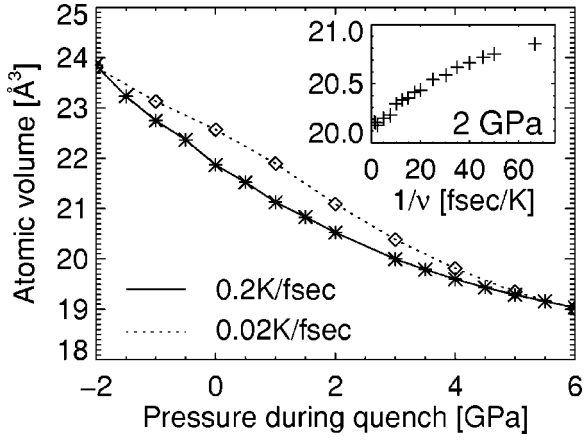

FIG. 4. Dependence of the atomic volume in *a*-*T*-Ge on the hydrostatic pressure and quench rate ν applied during passing the glass transition temperature.

lower pressures (higher viscosities). At quenching rates of 0.02 K/fsec, for instance, the glass transition temperatures are ≈2100 and ≈1200 K for pressures of 0 and 6 GPa, respectively. Only the 0 GPa case, moreover, shows strong tetrahedal coordination.

During further isobaric cooling below their respective glass transition temperatures, samples maintained at zero pressure continue to increase their tetrahedal coordination by forming a loose covalent network. This is reflected by a sharpening of the tetrahedal peak in the angular distribution, and it is accompanied by an anomalous increase in volume. With increasing pressure, the tendency for covalent bonding decreases, thus reducing the anomalous behavior of the system below the glass transition temperature (Fig. 4). In this sense, *a*-*T*-Ge, which is prepared at high pressures (typically 10 GPa), has a structure that is less covalent, and therefore in closer correspondence to the liquid state than is the glass

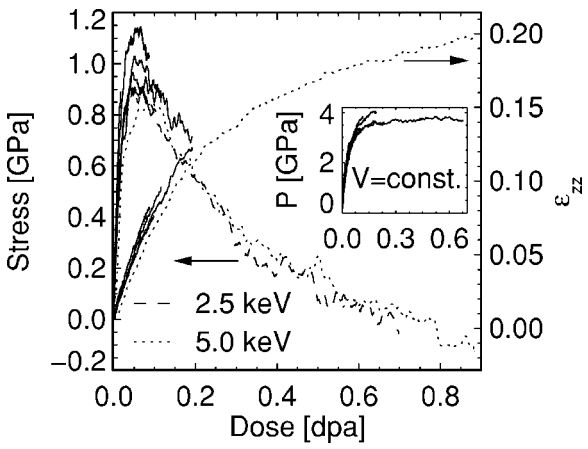

FIG. 5. MD simulations of recoil induced stresses, strains and pressures in an *a*-*T*-Ge simulation cell, using an open film (main plot) and constant volume (inset) geometry, respectively. For V =const, swelling leads to the generation of a hydrostatic pressure, whereas biaxial stresses and normal strains (ϵ_{zz}) are observed in the open film geometry. The various curves from the top to the bottom correspond to the recoil energies 10 eV, 50 eV, 100 eV, 300 eV, 500 eV, 1 keV, 2.5 keV, and 5 keV, respectively.

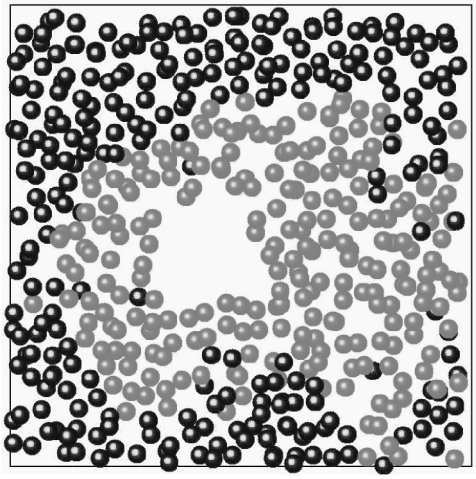

FIG. 6. In medium dense *a*-*T*-Ge, melting within thermal spikes (bright atoms) leads to large negative pressures (−3.1 GPa), and subsequent cavity formation—shown here 2 psec after starting a 5 keV recoil.

prepared at low pressures.[46] In this context we note that under isobaric conditions, *a*-*T*-Ge anomalously contracts on heating from 10 K to T_G for all pressures lower than ≈4 GPa, whereas it does not show this anomaly for higher pressures.

Irradiation simulations were performed on dense *a*-*T*-Ge cells, which were prepared by quenching at a rate of ν =0.02 K/fsec at P=4 GPa. These cells, therefore, were still strongly tetrahedally bonded. Shown in Fig. 5 as a function of dose are the results for the biaxial stress and strain for computational cells with an open film geometry and the hydrostatic pressure for cells employing the constant volume geometry (Fig. 5, inset). Several different recoil energies were considered. For the constant volume condition, the pressures saturate [P_{sat}(5.0 keV)≈3.7 GPa for *a*-*T*-Ge and P_{sat}(5.0 keV)≈2.5 GPa for *a*-SW-Ge] at high dose (0.2 and 0.15 dpa for *a*-*T*-Ge and *a*-SW-Ge, respectively). The lower saturation dose for *a*-SW-Ge can be explained, within a defect picture, on the basis of a lower displacement energy in the amorphous matrix (13 and 16 eV for *a*-SW-Ge and *a*-*T*-Ge, respectively). It can be explained within a thermal spike picture, moreover, by the lower glass temperature (and thus a more extended thermal spike). When bombardment takes place in the open film geometry, biaxial stresses are generated (Fig. 5). In contrast to the constant volume case, however, these stresses dissipate toward zero at high dose, owing to the swelling of the sample perpendicular to the open surface. The data illustrate that the pressures, stresses and swelling are largely independent of bombardment energy, when compared on the basis of deposited energy (or defect production), i.e., measured in dpa. The same conclusions are qualitatively valid for *a*-SW-Ge, although these samples show strongly reduced biaxial stresses (maximum: 0.19 GPa) and swelling (maximum: 5%). The lower recoil energies, moreover, show a small tendency for higher final pressures, stresses, and swelling.

A more atomistic view of the processes governing swelling and stress formation is provided in Fig. 6, where a cross

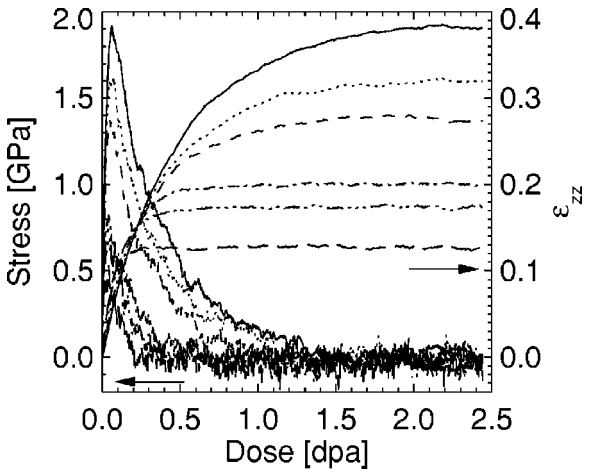

FIG. 7. Biaxial stresses and normal strains ϵ_{zz} during insertion of Frenckel pairs at various temperatures into a *a*-*T*-Ge cell in periodic film geometry: The curves for stresses and strains represent cells at temperatures of 10, 50, 100, 300, 500, and 800 K, from the top to the botton, respectively, i.e., the sample shows reduced swelling tendencies, the higher the temperature. Performing similar simulations using open film geometry results in statistically identical results, i.e., the results are independent from the presence or absence of a surface.

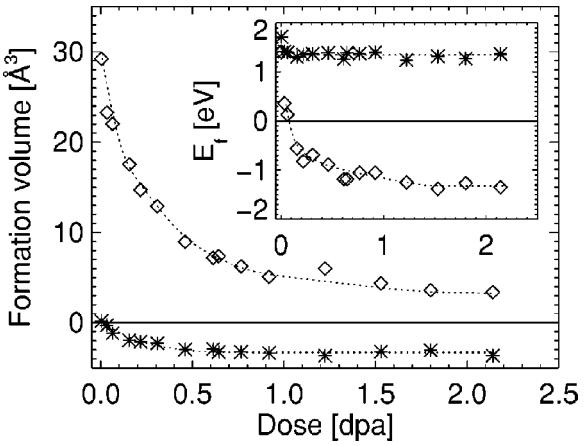

FIG. 8. Formation volumes and energies E_f for the creation of interstitials (diamonds) and vacancies (stars)—in dependence of the dose using a periodic film geometry.

sectional view of a 5 keV recoil event is shown in a medium-dense *a*-*T*-Ge. The location of the thermal-spike region is clearly identified after 2 psec. This region is under strong tensile stress and has a temperature close to T_G. During cooling below T_G, the material becomes structurally frozen, and it anomalously expands, as described above. Thus it preserves the cavity, while concurrently generating compressive stresses in the sample. The slight increase in swelling (represented by higher pressures, stresses and strain) observed at lower recoil energy, can be explained quite simply on the basis of a thermal spike mechanism. The higher the recoil energy, the longer the thermal spike persists, and hence the more the structure in the melt can relax under the condition of negative pressures. As discussed above, this yields a more open structure without creating pores (a similar effect is shown in the inset of Fig. 4 for the case of *positive* applied pressures).

Although this thermal-spike picture is an attractive explanation for swelling, it has some shortcomings. For example, our simulations indicate that this description is only valid for medium-dense *a*-*T*-Ge. At higher densities, no cavities are formed, whereas at too low densities, thermal spikes are not present, similar to the situation in crystalline semiconductors.[31] Additionally, our simulations indicate that at recoil energies as low as 20 eV swelling still occurs while local melting within a thermal spike does not. These various findings thus require a more generalized picture of swelling than that offered by the thermal spike model.

VI. POINT-DEFECT-INDUCED SWELLING

Since the thermal spike model appears inadequate to explain many of the simulation results, we examine whether the creation of point defects, in the absence of any thermal effects, can better account for the observed swelling behavior. We do this by inserting Frenkel pairs into *a*-*T*-Ge simulation cells at various temperatures. Statistically identical results are obtained for the open and periodic film geometries. Figure 7 presents the results for the periodic film geometry, which are characterized by the generation of high compressive stresses in the early stages of swelling, followed at higher doses by volume expansion, as characterized by ϵ_{zz}. A comparison between Frenkel pair insertion (Fig. 7) and recoil bombardment (Fig. 5), shows a remarkable similarity. Quantitative agreement is, in fact, found for the doses at which maximum stresses and volume expansion occur. The stress and strain levels obtained at 10 K during recoil bombardment, however, tend to be significantly smaller than they are for Frenkel pair insertion, also performed at 10 K. The comparison with Frenkel pair insertion performed at temperatures of 100–300 K yields much closer agreement. This suggests that swelling in recoil events is inherently connected with the creation of point defects during bombardment, but that concurrent thermal thermal relaxation effects around the defect reduce swelling. Recoil events are thus similar to the insertion of defects at a somewhat elevated temperature.

We further point out a striking connection between the point defects discussed within the current context, and the liquid region within a thermal spike in medium-dense *a*-*T*-Ge, as discussed in Sec. VI (especially Fig. 6). Our simulations clearly indicate that a liquid region is nearly structurally equivalent to highly covalently bonded *a*-*T*-Ge containing a high density of interstitials.

VII. MECHANISM OF SWELLING IN Ge

Before discussing how interstitial-like and vacancy-like defects give rise to irradiation-induced swelling, we first calculate the formation volumes and energies of these defects as a function of their concentration in differently prepared *a*-*T*-Ge simulation cells (Fig. 8). For vacancies we find a decrease in volume from zero, for unirradiated cells, to ≈ -3.5 Å^3, at high dose, and a constant formation energy of

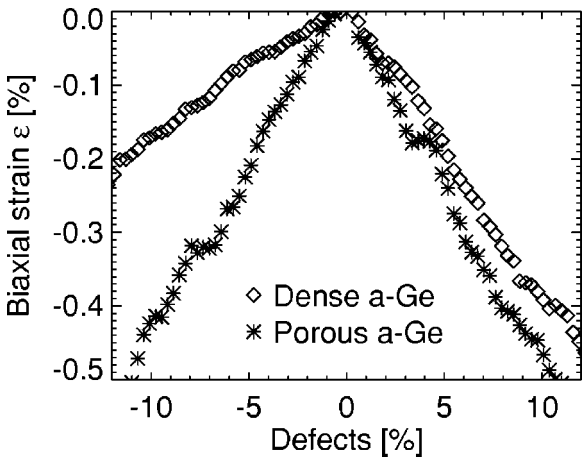

FIG. 9. Biaxial strains due to viscous flow caused by insertion of interstitials (positive defects) or vacencies (negative defects) into *as quenched* and irradiated (2.5 dpa Frenckel pairs) samples, respectively, using the periodic film geometry and biaxial compressive stresses (0.5 GPa).

≈1.4 eV. In contrast, the interstitials have a very high formation volume (≈29.5 Å^3) for unirradiated cells, which decreases by a factor of 10 to ≈3.5 Å^3 at high dose. The formation energy for interstitials anomalously switches from positive to negative values after a dose of only ≈0.1 dpa, i.e., interstitials become stable above this dose. In this context it is important to note that the relaxation volumes (defined as formation volume minus one atomic volume) of interstitials and vacancies follow curves that are proportional to the formation energy curve. The relaxation volume of interstitials, therefore, also anomalously turns negative for doses higher than ≈0.1 dpa, while staying constant for vacancies. The formation volumes and energies of Frenkel pairs are determined approximately by the sum of the corresponding individual contributions of vacancies and interstitials in Fig. 8, which both show a strong decrease from positive values towards zero at high enough doses. This is consistent with the observed swelling behavior shown in Fig. 7.

To better understand the present anomalies and their relation to swelling, we focus directly on the processes in the amorphous matrix that are caused by the creation of point defects. Previous studies on Lennard-Jones systems[40] have reported that interstitials relax more quickly into the amorphous structure than vacancies. Studies on metallic glasses, moreover, have found that relaxation upon insertion of interstitials and vacancies leads to *identical*[10] plastic flow under externally applied shear forcing. These results, however, are not guaranteed to hold in the presence of covalent bonding. The present studies thus focus exactly on this point by employing two different types of *a*-*T*-Ge samples, one unirradiated, and one that is loaded with 2.5 dpa of Frenkel pairs. During insertion of interstitials (positive defects) and vacancies (negative defects) the cells are subjected to shear stresses by externally applying a constant compressive biaxial stresses (0.5 GPa in *x* and *y* direction), while maintaining zero stress in the *z* direction. The plastic contributions to the biaxial strains are obtained by correcting for the defect formation volumes; the results are plotted in Fig. 9. In the as-quenched cell, the plastic deformation by interstitials is about a factor of 2 larger than that for vacancies, whereas in porous *a*-*T*-Ge, insertion of vacancies and interstitials yield approximately equal plastic flow. The corresponding radiation-induced fluiditities H for dense and porous cells are readily calculated from the slopes of the curves, $H=7.05\times10^{-10}$ and 1.15×10^{-9} (Pa dpa)$^{-1}$, respectively. (Fluidity is the inverse viscosity.) These values are in good agreement with the values that we previously reported for amorphous metals [$H\approx3\times10^{-9}$ (Pa dpa)$^{-1}$].[10]

The values for the radiation induced fluidities (Fig. 9) can be understood in terms of the defect formation volumes and energies (Fig. 8). In dense *a*-*T*-Ge, an inserted vacancy tends to enhance the local covalent bonding, and thus it stabilizes the region against volume change and shearing. This is reflected by a vanishing vacancy formation volume, as well as by a low vacancy-induced fluidity. With increasing porosity in the covalent network, however, the matrix is weakened, presumably due to the large number of missing bonds, and therefore can no longer resist volume changes and shear stresses. This leads to an increasingly negative formation volume and radiation induced fluidity. As the number of atomic bonds broken during insertion of the vacancy is approximately constant, the formation energy is independent of density. In contrast, self-interstitials are always severe deviations from a covalently bonded network. As discussed in Sec. VI, their local environment resembles liquid Ge or amorphous metals, with initially strongly reduced covalent bonding. Thus, a high orientational mobility develops, which easily responds to external shear forcing by viscous flow. Relaxation is achieved by the absorption of interstitials within the amorphous covalent network, accompanied by a volume change, which is essentially proportional to the density of the matrix, as seen from Figs. 7 and 8.

The above considerations identify the main ingredients of swelling. Once a Frenkel pair is created by ion bombardment in sufficiently dense *a*-Ge, the interstitial is rapidly absorbed in the amorphous matrix, since it reduces the covalent bonding and enables flow. The vacancy, on the other hand, maintains covalent bonding and remains localized. The delocalization of the interstitial coupled with a rigid vacancy, thus suppresses recombination. The excess volume, i.e., formation volume of the Frenkel pair, appears as pressure or stress. The stress, however, is eventually limited by interstitial-mediated viscous flow. It is noteworthy that *no* open surfaces are required for swelling or stress generation, in contrast to earlier assumptions. Swelling ceases, once the porosity is so high that all interstitials immediately recombine with nearby vacancies or voids.

VIII. COMPARISON OF EXPERIMENTS AND SIMULATIONS

A comparison of our experiments on ion induced stress generation (Sec. IV) with the MD simulations (Secs. V and VI) shows quantitatively similar compressive stress levels, which successively transform into swelling toward the open surface. On the other hand, stresses in the MD calculations

evolve at much lower doses than do the experiments and they relax towards zero stress at sufficiently high doses, whereas the experimental results do not. Finally, swelling in the simulations arrests but not in the experiments.

Part of the discrepancy between the simulations and experiments presumably derives from the different densities and structures in the vapor-deposited *a*-Ge films and the initial simulation cells. In fact, experimental studies of the morphology[36] show porosity in *as deposited* films, which, according to our simulations, will lead to reduced and slower stress generation than in initially dense *a*-Ge. This can account for the faster evolution of stress and higher values of stress in the simulations. The other discrepancy, viz. the continuous swelling observed in the experiments, is not directly accessible to MD studies, as we now discuss.

In agreement with our experimental findings, many previous works,[11–19] which primarily employed electron microscopy, reported enormous swelling and the formation of a cellular, spongelike structure. The incubation doses for these structures to form were as low as 2.8 dpa for ion energies between several tens of keV to several hundreds of MeV. Cell sizes in these structures ranged from several nanometers to $\approx$100 nm and densities decreased by as much as 70%, without showing signs of saturation. An important finding in two of these studies[12,19] for the present work, is that the spongelike structure does not form for irradiation temperatures $\lesssim$173 K, while showing more atomic-scale disorder at these temperatures.[41] Thus, continuous swelling requires thermal activation, and therefore it is unlikely to be captured in our MD simulations, owing to the short time scales accessible in MD modeling. In Sec. VII we noted that stress generation and swelling arrested in the MD simulations when the atomic level porosity became too large. Within the current context, it suggests that a similarly high atomic level porosity is not reached experimentally. We therefore conclude, that vacancy diffusion represents the thermally activated mechanism that is required for continuous swelling behavior. Once diffusion of vacancylike entities becomes possible, they will coalesce and form large cavities, leaving elsewhere a dense amorphous matrix. During further irradiation, interstitials can again be incorporated in the dense regions, as long as their distance to any nearby cavity is larger than the interstitial relaxation distance. These considerations make clear, that the only configurations that remain stable under ion bombardments consist of wall-like covalently bonded structures around the voids, with the uniform wall thickness equal to approximately the interstitial relaxation distance, and the dense, metallically bonded, amorphous regions between the walls that have low viscosities during irradiation. This behavior is quite similar to normal void swelling in crystals, interstitials preferentially go to sinks and enable changes in the dimensions of the sample, while vacancies migrate to voids.

The above explanation can also reasonably account for a reduced swelling in *a*-C and *a*-Si, as experimentally observed[42–44] The higher covalent character and strength, increasing from Ge to Si and C, leads to an increase in bond-orientational order and stabilization of vacancies—which results in more atomic scale porosity and thus increased interstitial-vacancy recombination and less swelling. The swelling behavior in Si and C, therefore, is similar to the low temperature regime of *a*-Ge.

IX. CONCLUSION

Radiation-induced stress generation and swelling were measured in *a*-Ge and modeled by MD simulations. This combined effort, along with previous studies, indicates that four factors play an important role in the observed phenomena. Ion bombardment creates Frenkel pair type of defects, but with only the vacancies remaining well localized. Interstitial-like defects mediate plastic flow; the value of the radiation-enhanced viscosity in *a*-Ge is similar to that in metallic glasses, suggesting the same mechanism. Diffusion of vacancies leads to cavity formation. Strong covalent bonding near vacancies and at cell walls suppresses recombination with interstitials. These studies thus bring new light into the mystery of Ge swelling, which has been the topic of debates for more than 20 years.

ACKNOWLEDGMENTS

The authors acknowledge grants of computer time by the National Energy Research Scientific Computing Center (NERSC), Gesellschaft für wissenschaftliche Datenverarbeitung Göttingen (GWDG), Germany and the National Center for Supercomputing Applications (NCSA). Financial support by the U.S. Dept. of Energy, Basic Energy Sciences, Grant No. DEFG02-91-ER45439, the Deutsche Forschungsgemeinschaft (DFG), Grant No. SFB 602, TP B3, and in part by the U.S. Dept. of Energy, and Nuclear Engineering Education Research (NEER) program under Grant No. DFG07-0l-ID14121 is gratefully acknowledged. Some of the experiments were carried out in the Center for Microanalysis of Materials, University of Illinois at Urbana-Champaign, which is partially supported by the U.S. Department of Energy under Grant No. DEFG02-91-ER45439.

*Electronic address: smayr@gwdg.de

[1] H. Bauer and W. Buckel, Z. Phys. **216**, 507 (1968).

[2] S. G. Mayr, in *Encyclopedia of Materials: Science and Technology*, edited by K. H. J. Buschow, R. W. Cahn, M. C. Flemings, B. Ilschner, E. J. Kramer, and S. Mahajan (Elsevier, Amsterdam, 2002).

[3] M. Moske and K. Samwer, Z. Phys. B: Condens. Matter **77**, 3 (1989).

[4] S. G. Mayr and K. Samwer, Phys. Rev. Lett. **87**, 036105 (2001).

[5] J. A. Floro, P. G. Kotula, S. C. Seel, and D. J. Srolovitz, Phys. Rev. Lett. **91**, 096101 (2003).

[6] S. G. Mayr and R. S. Averback, Phys. Rev. Lett. **87**, 196106

(2001).
[7] S. G. Mayr and R. S. Averback, Phys. Rev. B **68**, 214105 (2003).
[8] E. Snoeks, A. Polman, and C. A. Volkert, Appl. Phys. Lett. **65**, 2487 (1994).
[9] C. A. Volkert, J. Appl. Phys. **70**, 3521 (1991).
[10] S. G. Mayr, Y. Ashkenazy, K. Albe, and R. S. Averback, Phys. Rev. Lett. **90**, 055505 (2003).
[11] I. H. Wilson, J. Appl. Phys. **53**, 1698 (1981).
[12] B. R. Appleton, O. W. Holland, J. Narayan, O. E. Show, J. S. Williams, K. T. Short, and E. Lawson, Appl. Phys. Lett. **41**, 711 (1982).
[13] O. W. Holland, B. R. Appleton, and J. Narayan, J. Appl. Phys. **54**, 2295 (1983).
[14] L. M. Wang and R. C. Birtcher, Appl. Phys. Lett. **55**, 2494 (1989).
[15] L. M. Wang and R. C. Birtcher, Philos. Mag. A **64**, 1209 (1991).
[16] R. C. Birtcher, M. H. Grimsditch, and L. E. McNeil, Phys. Rev. B **50**, 8990 (1994).
[17] H. Huber *et al.*, Nucl. Instrum. Methods Phys. Res. B **122**, 542 (1997).
[18] Y. J. Chen, I. H. Wilson, W. Y. Cheung, J. B. Xu, and S. P. Wong, J. Vac. Sci. Technol. B **15**, 809 (1997).
[19] B. Stritzker, R. G. Elliman, and J. Zou, Nucl. Instrum. Methods Phys. Res. B **175–177**, 193 (2001).
[20] G. Stoney, Proc. R. Soc. London, Ser. A **82**, 172 (1909).
[21] S. G. Mayr and R. S. Averback, Phys. Rev. B **68**, 075419 (2003).
[22] J. F. Ziegler, J. P. Biersack, and U. Littmark, *The Stopping and Range of Ions in Matter* (Pergamon Press, New York, 1985).
[23] F. Evangelisti, M. Garozzo, and G. Conte, J. Appl. Phys. **53**, 7390 (1982).
[24] K. Nordlund and R. S. Averback, Phys. Rev. B **56**, 2421 (1997).
[25] J. Tersoff, Phys. Rev. B **38**, 9902 (1988).
[26] J. Tersoff, Phys. Rev. B **39**, 5566 (1989).
[27] H. Balamane, T. Halicioglu, and W. A. Tiller, Phys. Rev. B **46**, 2250 (1992).
[28] J. K. Bording, Phys. Rev. B **62**, 7103 (2000).
[29] F. H. Stillinger and T. A. Weber, Phys. Rev. B **31**, 5262 (1985).
[30] K. Ding and H. C. Andersen, Phys. Rev. B **34**, 6987 (1986).
[31] K. Nordlund, M. Ghaly, R. S. Averback, M. Catrula, T. D. de le Rubia, and J. Tarus, Phys. Rev. B **57**, 7556 (1998).
[32] I. Stich, R. Car, and M. Parinello, Phys. Rev. B **44**, 4262 (1991).
[33] H. J. C. Berendsen, J. P. M. Postma, W. F. van Gusteren, A. DiNola, and J. R. Haak, J. Chem. Phys. **81**, 3684 (1984).
[34] F. Seitz and J. Koehler, Solid State Phys. **2**, 305 (1956).
[35] R. S. Averback and T. D. de la Rubia, Solid State Phys. **51**, 281 (1998).
[36] T. M. Donovan and K. Heinemann, Phys. Rev. Lett. **27**, 1794 (1971).
[37] K. Tanaka, Phys. Rev. B **43**, 4302 (1991).
[38] F. X. Zhang and W. K. Wang, Phys. Rev. B **52**, 3113 (1995).
[39] M. Durandurdu and D. A. Drabold, Phys. Rev. B **66**, 041201 (2002).
[40] T. K. Chaki and J. C. M. Li, Philos. Mag. B **51**, 557 (1985).
[41] M. C. Ridgway, C. J. Glover, K. M. Yu, G. J. Foran, J. L. Hansen, and A. N. Larsen, Phys. Rev. B **61**, 12 586 (2000).
[42] J. F. Prins, T. E. Derry, and J. P. F. Sellschop, Phys. Rev. B **34**, 8870 (1986).
[43] D. N. Seidman, R. S. Averback, P. R. Okamoto, and A. C. Baily, Phys. Rev. Lett. **58**, 900 (1986).
[44] J. Fortner and J. S. Lannin, Phys. Rev. B **37**, 10 154 (1988).
[45] SRIM 2003 computer code (Ref. 22).
[46] It should be noted that at much higher pressures (≈20 GPa) a pressure induced phase transition occurs.